

# 1 **The subtle origins of surface-warming hiatuses**

2

3 Christopher Hedemann<sup>1,2\*</sup>, Thorsten Mauritsen<sup>1</sup>, Johann Jungclaus<sup>1</sup> and Jochem  
4 Marotzke<sup>1</sup>

5 <sup>1</sup> Max-Planck-Institut für Meteorologie, Bundesstraße 53, 20146 Hamburg, Germany

6 <sup>2</sup> International Max Planck Research School on Earth System Modelling, Max-  
7 Planck-Institut für Meteorologie, Bundesstraße 53, 20146 Hamburg, Germany

8 \*email: christopher.hedemann@mpimet.mpg.de

9

10 **During the first decade of the 21<sup>st</sup> Century, the Earth's surface warmed more**  
11 **slowly than climate models simulated<sup>1</sup>. This surface-warming hiatus is attributed**  
12 **by some studies to model errors in external forcing<sup>2-4</sup>, while others point to heat**  
13 **rearrangements in the ocean<sup>5-10</sup> caused by internal variability, the timing of**  
14 **which cannot be predicted by the models<sup>1</sup>. However, observational analyses**  
15 **disagree about which ocean region is responsible<sup>11-16</sup>. Here we show that the**  
16 **hiatus could also have been caused by internal variability in the top-of-**  
17 **atmosphere energy imbalance. Energy budgeting for the ocean surface layer**  
18 **over a 100-member historical ensemble reveals that hiatuses are caused by**  
19 **energy-flux deviations as small as 0.08 Wm<sup>-2</sup>, which can originate at the top of**  
20 **the atmosphere, in the ocean, or both. Budgeting with existing observations**  
21 **cannot constrain the origin of the recent hiatus, because the uncertainty in**  
22 **observations dwarfs the small flux deviations that could cause a hiatus. The**  
23 **sensitivity of these flux deviations to the observational dataset and to energy**  
24 **budget choices helps explain why previous studies conflict, and suggests that the**  
25 **origin of the recent hiatus may never be identified.**

26 The surface temperature of the Earth warmed more slowly over the period 1998–2012  
27 than could be expected by examining either most model projections or the long-term  
28 warming trend<sup>1</sup>. Even though some studies now attribute the deviation from the long-  
29 term trend to observational biases<sup>17,18</sup>, the gap between observations and models  
30 persists. The observed trend deviated by as much as –0.17 °C per decade from the  
31 CMIP5 (Coupled Model Intercomparison Project Phase 5; ref. 19) ensemble mean  
32 projection<sup>1</sup> – a gap two to four times the observed trend. The hiatus therefore  
33 continues to challenge climate science.

34 Many studies propose that heat was drawn down from the surface into deeper ocean  
35 layers by quasi-random decadal fluctuations known as internal variability. The trouble  
36 with this proposition is that most major ocean regions – the Pacific<sup>12,14</sup>, the Indian  
37 Ocean<sup>15</sup>, the Atlantic<sup>10</sup>, the Atlantic and the Southern Ocean<sup>13</sup>, and other  
38 combinations of basins<sup>5-7,11,16</sup> – have been named individually responsible for the  
39 heat uptake.

40 Here we explain these conflicting results and point to alternative interpretations. We  
41 develop a surface energy budget, which we apply to hiatuses in a 100-member  
42 historical ensemble (‘the large ensemble’), generated with the coupled climate model  
43 MPI-ESM1.1 (Methods; ref. 20). Using the surface energy budget, we quantify how  
44 much deviation in energy flux occurs during a hiatus. For each hiatus in the ensemble,  
45 we then determine its origin by quantifying energy contributions to the surface from  
46 the ocean and from the top-of-atmosphere (TOA) radiative imbalance (Supplementary  
47 Fig. 1). Finally, we use the energy budget to compare interpretations of the recent  
48 hiatus in existing observations<sup>9,21-23</sup>.

49 We define hiatuses in the large ensemble as any 15-year period where the GMST  
50 trend deviates by at least  $-0.17$  °C per decade from the ensemble mean. This  
51 definition is consistent with the gap between models and observations over the period  
52 1998–2012 (Fig. 1), as described in the Intergovernmental Panel on Climate Change  
53 Assessment Report 5 (ref. 1). Deviations in each ensemble member from the large-  
54 ensemble mean represent internal variability, which can be cleanly separated from the  
55 forced component (the ensemble mean) due to the ensemble’s unprecedented size.  
56 There are hundreds of such hiatuses (364, or 2.4% of all 15,200 trends) – subject to  
57 historical forcing but due entirely to internal variability – distributed across all time  
58 periods in the ensemble (Fig. 1).

59 The origin of each hiatus can be deduced from energy budgeting for the ocean’s  
60 surface layer (Supplementary Fig. 1), which dominates the thermal capacity of the  
61 Earth’s surface and therefore mediates the decadal GMST response to flux  
62 perturbations. We consider two main flux components acting on the ocean surface  
63 layer over decadal timescales: the TOA component from above and the ocean  
64 component from below (Fig. 2a). The TOA component is the top-of-atmosphere  
65 radiative flux imbalance minus atmospheric heat uptake. The ocean component is the  
66 total heat-content change below the ocean surface layer, defined at 100m depth. Both

67 components are converted to ensemble anomalies (to isolate the internal variability  
68 component) from values filtered over a 15-year sliding window (see Methods) and  
69 warm the surface layer when positive.

70 The budget is constructed this way for two reasons. Firstly, the chosen boundary  
71 fluxes (Fig. 2a) close the surface energy budget: the sum of the TOA component and  
72 ocean component highly correlates with heat-content changes within the ocean  
73 surface layer ( $r^2 = 0.97$ , slope=1.00; Supplementary Fig. 2). Other flux components  
74 (Fig. 2a) are excluded because they are small, are connected with known energy  
75 leakages, and because they do not improve budget closure (Methods; Supplementary  
76 Fig. 2b). The TOA imbalance and ocean heat uptake dominate decadal internal  
77 variability in the global energy budget of other CMIP5 models as well<sup>27</sup>. Secondly,  
78 the ocean surface layer is defined at 100m (as in refs. 24–26), because around this  
79 depth the flux-divergence anomaly for a hiatus reaches a maximum (Fig. 2b) and is  
80 therefore the most conservative choice for our analysis. Choosing a surface depth  
81 beyond 100m further exceeds the globally averaged mixed layer, and so the  
82 correlation between the energy budget and GMST trends sharply decays (Fig. 2b).

83 The energy budget allows us to determine the magnitude of flux anomalies associated  
84 with each hiatus. From the slope of the regression between surface-layer flux-  
85 divergence and GMST trends, we find that the expected flux-divergence anomaly for  
86 a hiatus (a  $-0.17$  °C per decade anomaly) is merely  $-0.082$   $\text{Wm}^{-2}$  (Methods). This  
87 corresponds to an average cooling over the ocean's top 100m of only  $-0.10$  °C per  
88 decade (Methods) but the effects of that cooling are amplified at the land surface<sup>28</sup>.  
89 Hiatuses caused only by the ocean tend to cool the land surface more effectively,  
90 which means they generally require a lower flux-divergence anomaly than other  
91 hiatuses to achieve the same cooling. Variation in the ratio of land to ocean surface-  
92 cooling leads to variation around the expected flux-divergence anomaly: an interval of  
93  $-0.082 \pm 0.038$   $\text{Wm}^{-2}$  covers the 5–95% range for all hiatuses. These results suggest  
94 that the total combined anomaly in TOA fluxes and ocean heat uptake that caused the  
95 gap between observations and models during the hiatus could be on the order of  $0.1$   
96  $\text{Wm}^{-2}$ . Defining hiatuses as equal to the observed 1998–2012 anomaly from the long-  
97 term observed trend (an anomaly of  $0.04$ – $0.07$  °C per decade) would reduce the  
98 threshold to just  $0.02$ – $0.03$   $\text{Wm}^{-2}$ .

99 Across the large ensemble, the  $0.082 \text{ Wm}^{-2}$  threshold in energy flux is frequently  
100 exceeded by anomalous heat-content changes in all major ocean basins, especially in  
101 the Atlantic, Pacific and Southern Oceans (Fig. 3b). However, these heat-content  
102 changes are dominated by interbasin heat exchange, which does not contribute to the  
103 surface-layer flux-divergence. In each major basin, the variations in heat content  
104 below the surface layer cannot predict trends in GMST (Fig. 3a), and indeed would  
105 falsely predict many more hiatuses than actually occur.

106 Even the global ocean heat uptake below 100m correlates poorly with GMST trends  
107 (Fig 3a). The TOA component tends to oppose the ocean component's contribution to  
108 the energy budget, as demonstrated by the negative correlation in Figure 3c. The flux-  
109 divergence anomaly, which has less than half the variability of either the TOA or  
110 ocean component alone (Fig. 3b), is the only reliable predictor of GMST trends (Fig.  
111 3a).

112 The role of the TOA and the ocean in each hiatus can be determined by comparing  
113 their relative contributions to the flux-divergence anomaly. For hiatuses in the large  
114 historical ensemble, the negative (cooling) anomaly is caused entirely by the TOA in  
115 12% of cases and by the ocean in 24%. In the remainder (64%), the negative anomaly  
116 is caused by the TOA and ocean acting together (bottom left quadrant of Fig. 3c).  
117 TOA variability is therefore involved in 76% of all hiatuses.

118 Applying a similar analysis to observations should reveal the energetic origin of the  
119 gap between models and observations during the recent hiatus (Supplementary Fig.  
120 1). We convert two observation-based estimates of fluxes over 2000–2010 to  
121 anomalies by subtracting the mean energy budget of the large ensemble for the same  
122 period (Methods). These anomalies include both the effect of internal variability and  
123 any potential effects of forcing differences between model and observations.

124 Choosing 2000–2010 means that we do not cover the full hiatus period (1998–2012)  
125 and that the corresponding gap in GMST trend between models and observations is  
126 reduced, because the warming rate increased after 2000 (ref. 18). However, this  
127 choice allows us to construct temporally consistent energy budgets from multiple  
128 sources and to take advantage of the improved quality of observations after 2000.  
129 Although the budgets do not cover the full hiatus period, they do illustrate how  
130 observational uncertainty affects interpretations of the hiatus. The first budget uses  
131 WOA ocean observations<sup>22</sup> and a recent estimate of TOA fluxes based on the CERES

132 satellite data product, Argo floats and AMIP simulations<sup>21</sup>. This first budget suggests  
133 that the hiatus was caused purely by the reduced influx of energy at the TOA (orange  
134 dot, Fig. 3c). The second budget, based on ocean reanalysis data from ORAS4 (refs.  
135 9,23), suggests the hiatus was caused purely by increased heat uptake in the ocean  
136 (green dot, Fig. 3c). The anomalies diagnosed from an ocean model forced with the  
137 exceptional Pacific trade winds observed during the hiatus<sup>12</sup> likewise suggest an  
138 ocean origin (purple dot, Fig. 3c).

139 From our analysis of observational estimates, we are unable to exclude the TOA  
140 anomaly as a possible cause of the recent hiatus. Referencing the observations to an  
141 alternative energy budget (rather than that of the large ensemble) could shift the  
142 absolute position of the green and orange crosses in Figure 3c. However, their relative  
143 distance from one another and the size of their error bars would not change.

144 Interpretations of the hiatus are also sensitive to the energy budgeting method used,  
145 and this may reveal why the results of previous studies conflict. For example, the  
146 hiatus has been explained as the result of heat being transferred from the surface  
147 ocean to the layers immediately below it, in the upper 300–350m (ref. 14, 16).

148 However, an energy budget that only accounts for heat exchange between the top  
149 100m and depths up to 300–350m correlates poorly with GMST trends in the large  
150 ensemble ( $r^2=0.08$ , Supplementary Fig. 4). A poor correlation also results when we  
151 exclude heat-content changes below the upper 700m ( $r^2=0.14$ , Supplementary Fig. 4;  
152 see ref. 15) and the upper 2000m of ocean ( $r^2=0.36$ , Supplementary Fig. 4; see ref.  
153 13). Heat-content changes up to as much as 4000m may be important for decadal  
154 internal variability (Supplementary Fig. 4), despite claims to the contrary<sup>16</sup>.

155 Furthermore, the pattern of surface-layer cooling overlying a warming trend may be  
156 common during ocean hiatuses, but it also occurs in around half of hiatuses caused  
157 purely by the TOA (Supplementary Fig. 5). During these TOA hiatuses, the  
158 subsurface warming is caused by heat transfer from deeper layers. Energy budgets  
159 that do not consider uptake across the whole ocean depth may therefore misrepresent  
160 crucial energy fluxes and misdiagnose the hiatus.

161 The hiatus may also be misdiagnosed by misrepresenting the surface layer in energy  
162 budgeting. For example, the surface layer has been defined at 300m ocean depth or  
163 more<sup>5,6,8–10,13</sup>. We perform energy budgeting in the large ensemble with a surface

164 layer that extends to 300m instead of 100m and find that the flux-divergence  
165 correlates comparatively poorly with GMST trends ( $r^2=0.33$  for 300m, Fig. 2b).

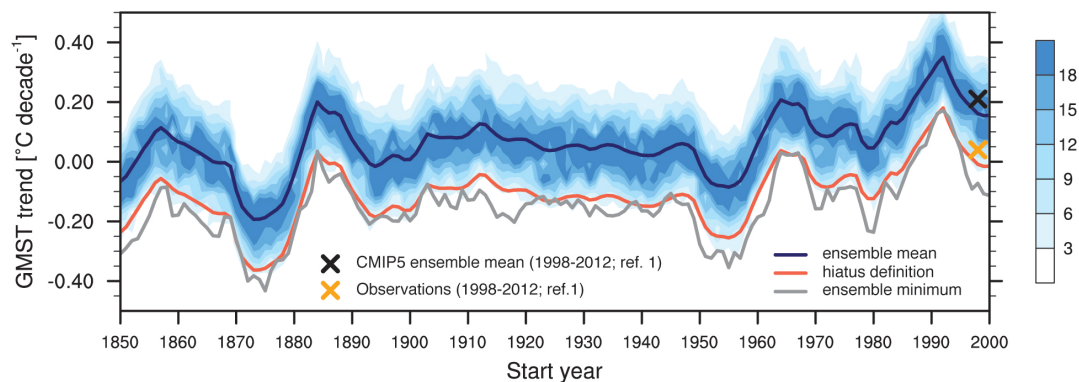
166 We conclude that the TOA may have been a source of significant internal variability  
167 during the hiatus. Our conclusions are not an artefact of model-generated TOA  
168 variability<sup>29</sup> – the large ensemble produces TOA variability that is similar to that in  
169 the observational record (Supplementary Fig. 6). Rather, our conclusions are based on  
170 a simple yet robust principle, namely that the Earth's surface layer has a small heat  
171 capacity. The surface temperature can therefore be influenced by small variations in  
172 the large yet mutually compensating fluxes that make up this layer's energy budget.  
173 Comparing the small variability in the TOA imbalance with the total TOA imbalance  
174 under global warming<sup>26,30</sup> obscures the significance of these small variations for the  
175 hiatus.

176 Other observational studies associate the hiatus with heat-flux anomalies that range  
177 from  $0.21 \text{ Wm}^{-2}$  (ref. 30) to  $0.50 \text{ Wm}^{-2}$  (ref. 11). But when we perform energy  
178 budgeting for the surface layer in the large ensemble, we find that anomalies closer to  
179  $0.08 \text{ Wm}^{-2}$  can account for hiatuses as large as  $0.17 \text{ }^\circ\text{C}$  per decade, and  $0.02\text{--}0.03$   
180  $\text{Wm}^{-2}$  for a hiatus equal to the 1998–2012 anomaly from the observed long-term  
181 trend. Because the flux-divergence anomaly is so small, ascribing the origin of the  
182 recent hiatus to the TOA or ocean requires that each of their contributions to the  
183 anomaly are known with considerable accuracy. However, the uncertainty in TOA  
184 imbalance from satellite measurements is two orders of magnitude larger ( $\sim 8 \text{ Wm}^{-2}$ ;  
185 ref. 31) than the anomaly we calculate. Satellite data are commonly anchored with  
186 ocean heat-content measurements, but the uncertainty range in TOA imbalance during  
187 the 2000s still remains around  $0.56 \text{ Wm}^{-2}$  (ref. 21), and even for the most recent  
188 estimate based on improved ocean observations over 2005–2015, the range is  $0.2$   
189  $\text{Wm}^{-2}$  (ref. 32).

190 This is the true dilemma at the heart of the hiatus debate: the variability in ocean heat  
191 content alone has no power to explain the hiatus, and the measure that can – the  
192 surface-layer flux-divergence – is dwarfed by observational uncertainty. While there  
193 are attempts to fill the gaps in observations with ocean reanalyses like ORAS4 (refs.  
194 9, 23), the resulting data are of questionable integrity during the hiatus<sup>14,21</sup> and, as we  
195 show, disagree with the budget based on CERES<sup>21</sup> and WOA<sup>22</sup>. Even if these  
196 disagreements could be reconciled, the process of anchoring satellite observations

197 with ocean heat uptake makes the contributions from TOA and ocean difficult to  
198 disentangle, because their absolute difference is unknown. Therefore, unless the  
199 uncertainty of observational estimates can be considerably reduced, the true origin of  
200 the recent hiatus may never be determined.

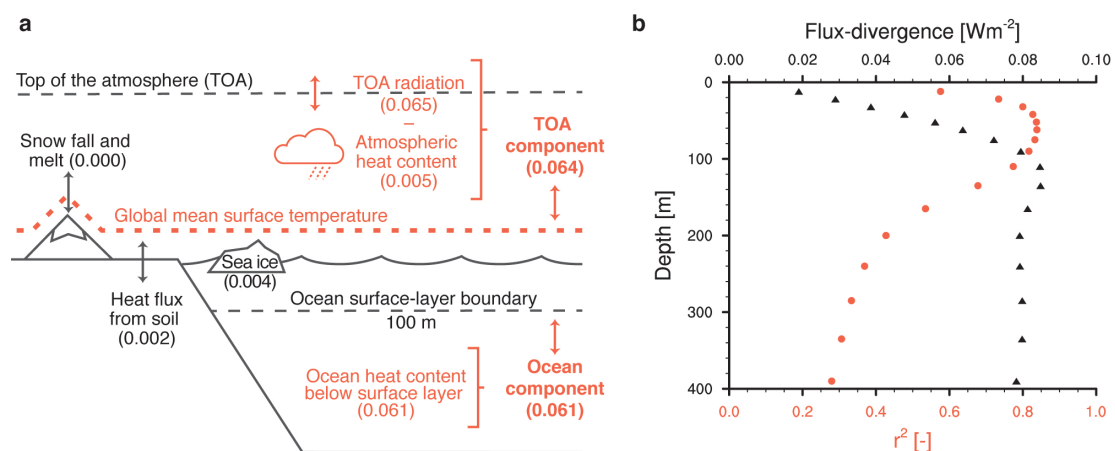
201

202 **Figures**

203

204 **Figure 1 | Distribution of 15-year trends in global mean surface temperature (GMST) in the 100-**  
 205 **member ensemble.** The coupled climate model MPI-ESM1.1 is forced with CMIP5-prescribed  
 206 historical forcing from 1850 until 2005, and extended until 2015 with the RCP4.5 scenario (see  
 207 Methods). When the red line lies above the grey line, at least one ensemble member is experiencing a  
 208 hiatus, defined as a deviation of more than 0.17 °C per decade below the ensemble mean. This  
 209 deviation is the same as the gap between the CMIP5 ensemble mean (black cross) and the observed  
 210 (yellow cross) GMST trends for the period 1998–2012. Contours represent the number of ensemble  
 211 members in bins of 0.05 °C per decade.

212

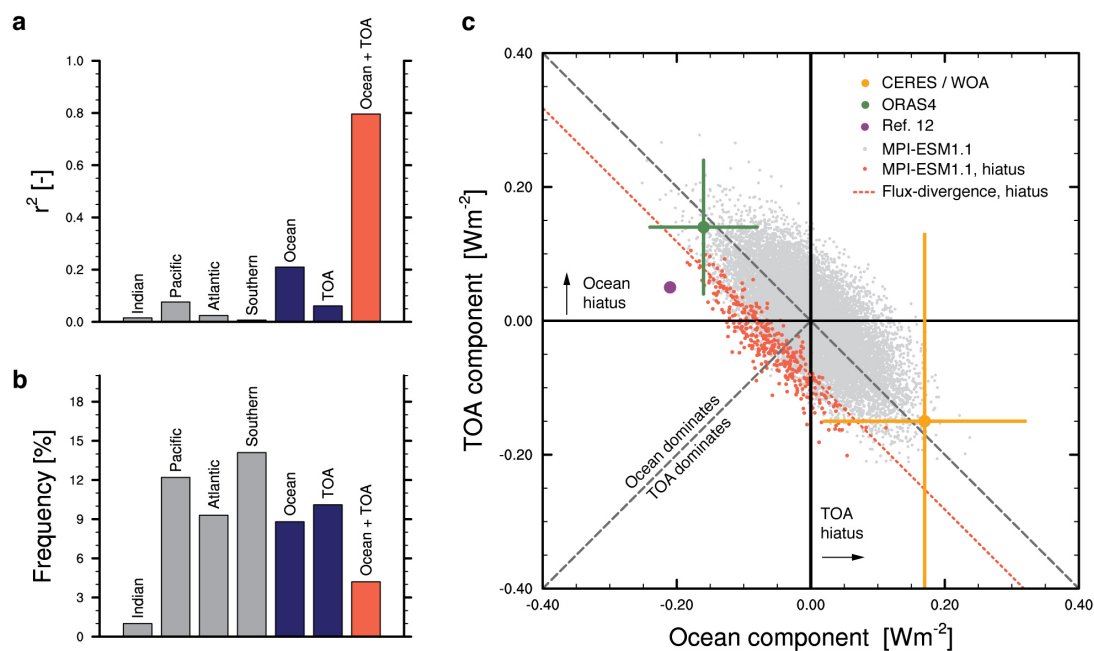


213

214 **Figure 2 | Surface energy budgets. a,** The surface energy budget in the large ensemble. Red colouring  
 215 indicates the global mean surface temperature (GMST) and the components included in the surface-  
 216 layer flux-divergence. The smaller flux components in black are excluded because they do not improve  
 217 budget closure or the relationship with GMST trends. Numbers in brackets represent the variability of  
 218 each heat flux ( $\text{Wm}^{-2}$ ), given as the root-mean-square of 15-year ensemble anomalies. **b,** Results from  
 219 surface budgets determined by increasingly deeper definitions of the ocean surface layer. For each  
 220 depth, a linear regression is performed for GMST trends against the surface-layer flux-divergence (both  
 221 as 15-year ensemble anomalies). Shown in black (top axis) is the expected deviation in flux-divergence  
 222 required to cause a hiatus, calculated from the regression slope. Shown in red (bottom axis) is the  
 223 correlation ( $r^2$ ) of each regression. The correlation rapidly deteriorates for definitions of the surface  
 224 layer below 100m.

225





226

227

228

229

230

231

232

233

234

235

236

237

238

239

240

241

242

**Figure 3 | Hiatuses and their origins in models and observations.** **a**, Correlation between global mean surface temperature (GMST) trends and heat fluxes in the large ensemble (as 15-year ensemble anomalies). **b**, Frequency with which each component exceeds the expected threshold for a hiatus ( $-0.082 \text{ Wm}^{-2}$ ). In **a** and **b**, grey bars represent changes in ocean heat content below the ocean surface layer (100m) by basin, blue bars represent the ocean and TOA components, and the red bar is the surface-layer flux-divergence (TOA + ocean components). **c**, Contributions to hiatuses from TOA and ocean components. Positive values indicate fluxes that warm the surface. Small red dots represent hiatuses in the large ensemble and small grey dots represent all other trends; the red dotted line is a flux-divergence of  $-0.082 \text{ Wm}^{-2}$ . Observational estimates and their 1-sigma error bars are compiled from multiple sources that rely either on CERES<sup>21</sup> and WOA data<sup>22</sup> (large orange dot) or ORAS4 data<sup>9,23</sup> (large green dot), shown as anomalies from the large-ensemble mean over the 2000s ( $-0.66 \text{ Wm}^{-2}$  for the ocean and  $+0.77 \text{ Wm}^{-2}$  for the TOA component). The large purple dot represents results from an ocean model forced with reanalysis-based winds as reported in ref. 12, converted to mean fluxes over 15 years.

## References

243

244

245

246

247

248

249

250

251

252

253

254

255

256

1. Flato, G. *et al.* in *Climate Change 2013: The Physical Science Basis*. (eds. Stocker, T. F. *et al.*) 741–866 (Cambridge University Press, 2013).
2. Solomon, S. *et al.* The persistently variable ‘background’ stratospheric aerosol layer and global climate change. *Science* **333**, 866–870 (2011).
3. Santer, B. D. *et al.* Volcanic contribution to decadal changes in tropospheric temperature. *Nat. Geosci.* **7**, 185–189 (2014).
4. Kopp, G. & Lean, J. L. A new, lower value of total solar irradiance: Evidence and climate significance. *Geophys. Res. Lett.* **38**, 1–7 (2011).
5. Meehl, G. A., Arblaster, J. M., Fasullo, J. T., Hu, A. & Trenberth, K. E. Model-based evidence of deep-ocean heat uptake during surface-temperature hiatus periods. *Nat. Clim. Chang.* **1**, 360–364 (2011).
6. Meehl, G. A., Hu, A., Arblaster, J. M., Fasullo, J. & Trenberth, K. E. Externally Forced and Internally Generated Decadal Climate Variability Associated with the Interdecadal Pacific Oscillation. *J. Clim.* **26**, 7298–7310

- 257 (2013).
- 258 7. Guemas, V., Doblas-Reyes, F. J., Andreu-Burillo, I. & Asif, M. Retrospective  
259 prediction of the global warming slowdown in the past decade. *Nat. Clim.*  
260 *Chang.* **3**, 649–653 (2013).
- 261 8. Watanabe, M. *et al.* Strengthening of ocean heat uptake efficiency associated  
262 with the recent climate hiatus. *Geophys. Res. Lett.* **40**, 3175–3179 (2013).
- 263 9. Balmaseda, M. A., Trenberth, K. E. & Källén, E. Distinctive climate signals in  
264 reanalysis of global ocean heat content. *Geophys. Res. Lett.* **40**, 1754–1759  
265 (2013).
- 266 10. Katsman, C. A. & van Oldenborgh, G. J. Tracing the upper ocean’s ‘missing  
267 heat’. *Geophys. Res. Lett.* **38**, (2011).
- 268 11. Drijfhout, S. S. *et al.* Surface warming hiatus caused by increased heat uptake  
269 across multiple ocean basins. *Geophys. Res. Lett.* **41**, 7868–7874 (2014).
- 270 12. England, M. H. *et al.* Recent intensification of wind-driven circulation in the  
271 Pacific and the ongoing warming hiatus. *Nat. Clim. Chang.* **4**, 222–227 (2014).
- 272 13. Chen, X. & Tung, K.-K. Varying planetary heat sink led to global-warming  
273 slowdown and acceleration. *Science* **345**, 897–903 (2014).
- 274 14. Nieves, V., Willis, J. K. & Patzert, W. C. Recent hiatus caused by decadal shift  
275 in Indo-Pacific heating. *Science* **349**, 532–535 (2015).
- 276 15. Lee, S.-K. *et al.* Pacific origin of the abrupt increase in Indian Ocean heat  
277 content during the warming hiatus. *Nat. Geosci.* **8**, (2015).
- 278 16. Liu, W., Xie, S.-P. & Lu, J. Tracking ocean heat uptake during the surface  
279 warming hiatus. *Nat. Commun.* **7**:10926 (2016).
- 280 17. Cowtan, K. & Way, R. G. Coverage bias in the HadCRUT4 temperature series  
281 and its impact on recent temperature trends. *Q. J. R. Meteorol. Soc.* **140**, 1935–  
282 1944 (2014).
- 283 18. Karl, T. R. *et al.* Possible artifacts of data biases in the recent global surface  
284 warming hiatus. *Science* **348**, 1469–72 (2015).
- 285 19. Taylor, K. E., Stouffer, R. J. & Meehl, G. a. An overview of CMIP5 and the  
286 experiment design. *Bull. Am. Meteorol. Soc.* **93**, 485–498 (2012).
- 287 20. Giorgetta, M. a. *et al.* Climate and carbon cycle changes from 1850 to 2100 in  
288 MPI-ESM simulations for the Coupled Model Intercomparison Project phase 5.  
289 *J. Adv. Model. Earth Syst.* **5**, 572–597 (2013).
- 290 21. Smith, D. M. *et al.* Earth’s energy imbalance since 1960 in observations and  
291 CMIP5 models. *Geophys. Res. Lett.* **42**, 1205–1213 (2015).
- 292 22. Levitus, S. *et al.* World ocean heat content and thermosteric sea level change  
293 (0–2000 m), 1955–2010. *Geophys. Res. Lett.* **39**, (2012).
- 294 23. Trenberth, K. E., Fasullo, J. T. & Balmaseda, M. A. Earth’s Energy Imbalance.  
295 *J. Clim.* **27**, 3129–3144 (2014).
- 296 24. Baker, M. B. & Roe, G. H. The shape of things to come: Why is climate  
297 change so predictable? *J. Clim.* **22**, 4574–4589 (2009).
- 298 25. Geoffroy, O. *et al.* Transient climate response in a two-layer energy-balance

- 299 model. Part I: Analytical solution and parameter calibration using CMIP5  
300 AOGCM experiments. *J. Clim.* **26**, 1841–1857 (2013).
- 301 26. Brown, P. T., Li, W., Li, L. & Ming, Y. Top-of-atmosphere radiative  
302 contribution to unforced decadal global temperature variability in climate  
303 models. *Geophys. Res. Lett.* **41**, 5175–5183 (2014).
- 304 27. Palmer, M. D. & McNeall, D. J. Internal variability of Earth’s energy budget  
305 simulated by CMIP5 climate models. *Environ. Res. Lett.* **9**, 034016 (2014).
- 306 28. Byrne, P. B. & O’Gorman, P. A. Land-ocean warming contrast over a wide  
307 range of climates: Convective quasi-equilibrium theory and idealized  
308 simulations. *J. Clim.* **26**, 4000–4016 (2013).
- 309 29. Stephens, G. L. *et al.* The albedo of Earth. *Rev. Geophys.* **53**, 141–163 (2015).
- 310 30. Trenberth, K. E. & Fasullo, J. T. An apparent hiatus in global warming?  
311 *Earth’s Future.* **1**, 19–32 (2013).
- 312 31. Loeb, N. G. *et al.* Toward optimal closure of the Earth’s top-of-atmosphere  
313 radiation budget. *J. Clim.* **22**, 748–766 (2009).
- 314 32. Johnson, G. C., Lyman, J. M. & Loeb, N. G. Improving estimates of Earth’s  
315 energy imbalance. *Nat. Clim. Chang.* **6**, 639–640 (2016).

316

### 317 **Corresponding author**

318 Correspondence to: Christopher Hedemann

### 319 **Acknowledgements**

320 This work is supported by the Max Planck Society for the Advancement of Science  
321 through the International Max Planck Research School on Earth System Modelling  
322 (IMPRS-ESM). J.J. acknowledges support from the European Union’s Horizon 2020  
323 research and innovation programme (grant agreement n° 633211). We thank Helmuth  
324 Haak for his technical assistance, Hao Zuo and Drew Peterson for providing the  
325 NEMO grid configuration, and Bjorn Stevens and Chao Li for their comments on the  
326 manuscript. We are indebted to Luis Kornbluh for producing the large historical  
327 ensemble and to Thomas Schulthess and the Swiss National Computing Centre  
328 (CSCS) for providing the necessary computational resources. Thanks also to Jürgen  
329 Kröger for producing the RCP4.5 extensions with the Deutsches Klimarechenzentrum  
330 (DKRZ) facilities.

### 331 **Author contributions**

332 C.H. and J.M. conceived the original idea for this study. C.H. developed the  
333 methodology and performed the analysis. All authors discussed the results. C.H.  
334 wrote the manuscript with input from J.M., T.M. and J.J.

### 335 **Competing financial interests**

336 The authors declare no competing financial interests.

337

## 338 **Methods**

339 The large historical ensemble in this study was generated by the Max Planck Institute  
340 Earth System Model version 1.1 (MPI-ESM1.1), an incremental improvement of the  
341 coupled ocean-atmosphere general circulation model submitted to CMIP5 in the LR  
342 configuration<sup>20</sup>. The 100 ensemble members were generated under CMIP5 historical  
343 forcing from 1850 until 2005, with extensions to 2015 under the RCP4.5 scenario<sup>20</sup>.  
344 The ensemble's internal variability of 15-year GMST trends (5–95% range of 0.30 °C  
345 per decade) is slightly larger than an estimate for the CMIP5 ensemble (5–95% range  
346 of 0.26 °C per decade; ref. 33).

347 GMST trends are calculated from the slope of an ordinary least-squares linear  
348 regression over a 15-year sliding window, to be consistent with the hiatus as  
349 described in ref. 1. Ensemble anomalies are then calculated at each time step:

$$350 \quad X'_{t,n} = X_{t,n} - \frac{1}{100} \sum_{n=1}^{100} X_{t,n}, \text{ where } t \text{ is the time-step and } n \text{ is the ensemble member.}$$

351 The composition of the energy budget is chosen to maximise the correlation of the  
352 surface-layer flux-divergence with both GMST trends and changes in ocean surface-  
353 layer heat content.

354 For the comparison with GMST trends (Supplementary Fig. 2) and most of this study,  
355 any terms expressed as heat content (Joules) are converted to trend anomalies in the  
356 same way as GMST, and then converted to units of  $\text{Wm}^{-2}$  over the total surface area  
357 of the Earth. All energy fluxes that are output from the model as  $\text{Wm}^{-2}$  are first time-  
358 integrated and then treated the same as heat content. This step ensures the same time-  
359 filtering for all aspects of the energy budget, and thereby prevents the introduction of  
360 significant errors. In the case of the net TOA imbalance, an energy-leakage constant  
361 of  $0.44 \text{ Wm}^{-2}$  is first estimated from 2000 years of the control run and then removed.  
362 Leakage is energy destroyed by model errors; MPI-ESM1.1 has improved energy  
363 conservation compared to its predecessor, MPI-ESM, and both have relatively small  
364 leakage compared to models in the CMIP5 ensemble<sup>34</sup>.

365 The comparison between flux-divergence and ocean surface-layer heat content  
366 (Supplementary Fig. 1) uses a slightly different approach. To test for exact changes in  
367 heat content over a 15-year period, only the start and end states are relevant. The  
368 least-squares method is however, influenced by the pathway from start- to end-states.

369 Instead, a difference filter is calculated from the start- and end-years in the 15-year  
370 sliding window, divided by the time difference of 14 years:  $\Delta X_t = \frac{1}{14}(X_{t+14} - X_t)$ .

371 The selected flux-divergence is the sum of two components: the TOA radiative  
372 imbalance minus atmospheric heat uptake (trends in vertically integrated moist static  
373 energy); and trends in ocean heat content below the ocean surface layer. This is the  
374 simplest flux combination that matches the expected one-to-one relationship between  
375 flux-divergence and change in surface-layer heat content (Supplementary Fig. 1). The  
376 salient characteristic of the ocean surface layer for this study is the relationship  
377 between heat-content changes within the layer and resulting changes in GMST. The  
378 surface-layer depth of 100m is therefore chosen to maintain the high correlation  
379 between the flux-divergence and GMST trends (Fig. 2b), but remains a conservative  
380 choice for estimation of the flux-divergence threshold during hiatuses. Removing heat  
381 changes that are related to phase changes (land-ice and sea-ice changes) or including  
382 the heat flux from the soil does not improve the relationship with GMST trends  
383 (Supplementary Fig. 2).

384 The expected surface-layer flux-divergence associated with a hiatus is calculated from  
385 the slope of the regression between flux-divergence and GMST trends. The value we  
386 calculate ( $-0.082 \text{ Wm}^{-2}$ ) is less than the flux-divergence required by uniform cooling  
387 of  $-0.17 \text{ }^\circ\text{C}$  per decade in the top 100m of ocean:  $-0.150 \text{ Wm}^{-2}$ . This is because the  
388 layer cools on average by only  $-0.10 \text{ }^\circ\text{C}$  per decade during hiatuses, which matches  
389 the theoretically expected cooling if the total anomaly of  $-0.082 \text{ Wm}^{-2}$  were focussed  
390 in the ocean surface layer. The error interval of  $\pm 0.038 \text{ Wm}^{-2}$  is calculated from the 5-  
391 95% range of all regression residuals of flux-divergence during hiatuses in the  
392 ensemble. There is no significant relationship between the origin of hiatuses and  
393 different periods in time (Supplementary Table 2).

394 The heat-content changes for individual basins are calculated from linear trends in  
395 heat content below 100m. Basin boundaries are identical to those used in CMIP5 and  
396 can be downloaded from the quality-control data in ref. 35.

397 Observational estimates in Figure 3c rely on a combination of data sources, which are  
398 summarised below and quantified in Supplementary Table 1. The CERES/WOA  
399 estimate for the 2000s is composed from the estimate of TOA fluxes in ref. 21, and an  
400 estimate of heat uptake using WOA data<sup>22</sup>, including pentadal heat-content values for

401 700m–2000m, yearly heat content values for the upper 700m, and a separate estimate  
402 for deep-ocean warming<sup>36</sup>. From the total heat uptake, we subtract the heat-content  
403 trend for the first 100m in the WOA objective analysis data<sup>22</sup> (calculated from in-situ  
404 temperature with a constant density and specific heat of  $4 \times 10^6$  Joules  $\text{m}^{-3} \text{°C}^{-1}$ ).

405 For this first budget, the 1-sigma error bars for the TOA estimate are taken from the  
406 same source as the estimate itself<sup>21</sup>. The error bars for the WOA ocean heat-content  
407 trend are calculated as plus or minus the standard error of the slope parameter,  
408 assuming that the errors in heat content are auto-correlated and behave like an AR(1)  
409 process<sup>37,38</sup>. The auto-correlation coefficient for the errors is estimated from residuals  
410 in heat-content data preceding the 2000s (1957-1999). A reduced degrees-of-freedom  
411 is calculated from the auto-correlation coefficient and scales the estimate of the  
412 standard error in heat content, which is calculated directly from the error estimates  
413 provided with the WOA data<sup>22</sup> (not from the regression residuals).

414 The ORAS4 ocean anomaly is calculated using an estimate for the total-depth heat  
415 uptake in the 2000s (ref. 9) minus the trend for the top 100m, which is calculated  
416 from the available ORAS4 potential temperature values with a constant density and  
417 specific heat of  $4 \times 10^6$  Joules  $\text{m}^{-3} \text{°C}^{-1}$ . The 1-sigma error bars are taken directly from  
418 ref. 9. For this second budget, the corresponding TOA flux estimate and its error bars  
419 are taken from ref. 23.

420 For both observation-based budgets, we remove the effect of ocean drift in the large  
421 ensemble. A quadratic function is first fitted to ocean heat content over the 2000-year  
422 control run<sup>39</sup>. Since each ensemble member starts from a different point in the control  
423 run, the drift is estimated from the rate-of-change in the quadratic that corresponds to  
424 each ensemble member's midpoint. The resulting ensemble-mean drift of  $0.01 \text{ Wm}^{-2}$   
425 is removed from both the ocean component and the TOA component.

426 In ref. 12, the budget is given as anomalies from the control experiment in total heat-  
427 content change for the top 125m of ocean and the remaining ocean. We convert these  
428 values to 15-year fluxes over the total Earth surface. We assume that the anomaly  
429 below 125m represents the ocean component, and the sum of surface and deep-ocean  
430 components is equivalent to the TOA component.

431

432 **Code availability.** The MPI-ESM1.1 model version was used to generate the large  
 433 ensemble and is available at [http://www.mpimet.mpg.de/en/science/models/mpi-  
 435 esm.html](http://www.mpimet.mpg.de/en/science/models/mpi-<br/>
  434 esm.html). Computer code used in post-processing of raw data has been deposited with  
 436 the Max Planck Society:  
 437 <http://pubman.mpd.l.mpg.de/pubman/faces/viewItemFullPage.jsp?itemId=escidoc:2353695>.

438 **Data availability.** Raw data from the large ensemble were generated at the Swiss  
 439 National Computing Centre (CSCS) and Deutsches Klimarechenzentrum (DKRZ)  
 440 facilities. Derived data have been deposited with the Max Planck Society  
 441 (<http://pubman.mpd.l.mpg.de/pubman/faces/viewItemFullPage.jsp?itemId=escidoc:2353695>).  
 442 Supplementary Figure 6 uses TOA flux reconstructions provided by R  
 443 Allan<sup>40</sup> (<http://www.met.reading.ac.uk/~sgs01c1l/flux/>) and satellite observations  
 444 provided by the NASA CERES project<sup>31</sup> (<http://ceres.larc.nasa.gov>). For  
 445 observational estimates in Figure 3c, we make use of data provided by the NOAA  
 446 World Ocean Atlas<sup>22</sup> ([https://www.nodc.noaa.gov/OC5/3M\\_HEAT\\_CONTENT/](https://www.nodc.noaa.gov/OC5/3M_HEAT_CONTENT/)) and  
 447 by the ECMWF Ocean Reanalysis System 4 (ref. 9;  
 448 <http://icdc.zmaw.de/projekte/easy-init/easy-init-ocean.html>).

449

## 450 References

- 451 33. Marotzke, J. & Forster, P. M. Forcing, feedback and internal variability in  
 452 global temperature trends. *Nature* **517**, 565–570 (2014).
- 453 34. Mauritsen, T. *et al.* Tuning the climate of a global model. *J. Adv. Model. Earth*  
 454 *Syst.* **4**, (2012).
- 455 35. Jungclaus, J. *et al.* CMIP5 simulations of the Max Planck Institute for  
 456 Meteorology (MPI-M) based on the MPI-ESM-LR model: The decadal2000  
 457 experiment, served by ESGF. World Data Center for Climate (WDCC) at  
 458 DKRZ. <http://dx.doi.org/doi:10.1594/WDCC/CMIP5.MXEL00> (2013).
- 459 36. Purkey, S. G. & Johnson, G. C. Warming of global abyssal and deep Southern  
 460 Ocean waters between the 1990s and 2000s: Contributions to global heat and  
 461 sea level rise budgets. *J. Clim.* **23**, 6336–6351 (2010).
- 462 37. Hartmann, D. L. *et al.* in *Climate Change 2013: The Physical Science Basis*.  
 463 (eds. Stocker, T. F. *et al.*) 2SM-1–2SM-30 (Cambridge University Press, 2013).
- 464 38. Santer, B. D. *et al.* Consistency of modelled and observed temperature trends  
 465 in the tropical troposphere. *Int. J. Climatol.* **28**, 1703–1722 (2008).
- 466 39. Sen Gupta, A., Jourdain, N. C., Brown, J. N. & Monselesan, D. Climate drift in  
 467 the CMIP5 models. *J. Clim.* **26**, 8597–8615 (2013).

- 468 40. Allan, R. P. *et al.* Changes in global net radiative imbalance 1985 – 2012.  
469 *Geophys. Res. Lett.* **41**, 5588–5598 (2014)